

Model-independent cosmic acceleration and type Ia supernovae intrinsic luminosity redshift dependence

I. Tutusaus¹, B. Lamine¹, and A. Blanchard¹

IRAP, Université de Toulouse, CNRS, CNES, UPS, (Toulouse), France
e-mail: isaac.tutusaus@irap.omp.eu

Received –; accepted –

ABSTRACT

Context. The Λ CDM model is the current standard model in cosmology thanks to its ability to reproduce the observations. The first observational evidence for this model appeared roughly 20 years ago from the type Ia supernovae (SNIa) Hubble diagram from two different groups. However, there has been some debate in the literature concerning the statistical treatment of SNIa, and their ability to prove the cosmic acceleration.

Aims. In this paper we relax the standard assumption that SNIa intrinsic luminosity is independent of the redshift, and we examine whether it may have an impact on our cosmological knowledge; more precisely, on the accelerated nature of the expansion of the Universe.

Methods. In order to be as general as possible, we do not specify a given cosmological model, but we reconstruct the expansion rate of the Universe through a cubic spline interpolation fitting the observations of the different cosmological probes: SNIa, baryon acoustic oscillations (BAO), and the high-redshift information from the cosmic microwave background (CMB).

Results. We show that when SNIa intrinsic luminosity is not allowed to vary as a function of the redshift, cosmic acceleration is definitely proven in a model-independent approach. However, allowing for a redshift dependence, a non-accelerated reconstruction of the expansion rate is able to fit, as well as Λ CDM, the combination of SNIa and BAO data, both treating the BAO standard ruler r_d as a free parameter (not entering on the physics governing the BAO), or adding the recently published prior from CMB observations. We further extend the analysis by including the CMB data. In this case we also consider a third way to combine the different probes by explicitly computing r_d from the early Universe physics, and we show that a non-accelerated reconstruction is able to nicely fit this combination of low and high-redshift data. We also check that this reconstruction is compatible with the latest measurements of the growth rate of matter perturbations. We finally show that the value of the Hubble constant (H_0) predicted by this reconstruction is in tension with model-independent measurements.

Conclusions. We present a model-independent reconstruction of a non-accelerated expansion rate of the Universe that is able to nicely fit all the main background cosmological probes. However, the predicted value of H_0 is in tension with recent direct measurements. Our analysis points out that a final, reliable, and consensual value for H_0 would be critical to definitively prove the cosmic acceleration in a model-independent way.

Key words. cosmology: observations – cosmological parameters – supernovae: individual: SNIa luminosity evolution

1. Introduction

The cosmological concordance model (Λ CDM), mainly composed of cold dark matter and dark energy, provides an extremely precise description of the properties of our Universe with very few parameters. However, recent observations [Planck Collaboration et al. (2016a); Betoule et al. (2014); Beutler et al. (2011)] show that these components form about 95% of the energy content of the Universe, and their true nature remain still unknown. The evidence for an accelerated expansion, coming from the type Ia supernovae (SNIa) Hubble diagram [Riess et al. (1998); Perlmutter et al. (1999)], was key to consider the Λ CDM as the concordance model. But there has recently been a debate in the literature wondering whether SNIa data alone, or combined with other low-redshift cosmological probes, can prove the accelerated expansion of the Universe [Nielsen et al. (2016); Shariff et al. (2016); Rubin & Hayden (2016); Ringermacher & Mead (2016); Tutusaus et al. (2017); Dam et al. (2017); Lonappan et al. (2017); Haridasu et al. (2017); Lin et al. (2017); Luković et al. (2018)]. For instance, the authors in Nielsen et al. (2016) claim that, allowing for the varying shape of the light curve and ex-

inction by dust, they find that SNIa data are still quite consistent with a constant rate of expansion, while the authors in Rubin & Hayden (2016) claim, redoing this analysis, a 11.2σ confidence level for acceleration with SNIa data alone in a flat universe.

In SNIa analyses it is usually assumed that two different SNIa in two different galaxies with the same colour, stretch of the light-curve, and host stellar mass, have on average the same intrinsic luminosity, independently of the redshift. In this work we follow the approach of our previous analysis [Tutusaus et al. (2017)], and we relax this assumption by allowing these SNIa to have different intrinsic luminosities as a function of the redshift. Relaxing this redshift independence assumption has also been considered in other analyses [Wright (2002); Drell et al. (2000); Linden et al. (2009); Nordin et al. (2008); Ferramacho et al. (2009)]. In Tutusaus et al. (2017) it was shown that a non-accelerated power law cosmology was able to fit the main low-redshift cosmological probes: SNIa, the baryon acoustic oscillations (BAO), the Hubble parameter as a function of the redshift ($H(z)$), and measurements of the growth of structures ($f\sigma_8(z)$), when some intrinsic luminosity redshift dependence is allowed. Nevertheless, this specific power-law model is excluded when

considering cosmic microwave background (CMB) information (as it was shown in [Tutusaus et al. (2016)]), and recently confirmed by the authors of Riess et al. (2018), who showed that such a model cannot fit the latest SNIa observations at $z > 1$, even when accounting for some luminosity evolution. In this paper we extend our previous study with a model-independent analysis, and we include the latest BAO observations as well as the complementary high-redshift CMB data. In order to be as general as possible, we follow the approach of Bernal et al. (2016) and reconstruct the expansion rate at late times through a cubic spline interpolation.

In Sect. 2 we present the different cosmological probes and the specific data sets considered in the analysis. In Sect. 3 we describe the methodology used to reconstruct the expansion rate in a model-independent way. We provide the results of our study in Sect. 4, and we conclude in Sect. 5.

2. Cosmological probes

In this section we present the different cosmological probes considered in the analysis, as well as the specific data sets used.

2.1. Type Ia supernovae

Type Ia supernovae are considered standardizable candles and they are useful to measure cosmological distances and break some degeneracies present in other cosmological probes. The standard observable used in SNIa measurements is the so-called distance modulus,

$$\mu(z) = 5 \log_{10} \left(\frac{H_0}{c} d_L(z) \right), \quad (1)$$

where $d_L(z) = (1+z)r(z)$ is the luminosity distance, and $r(z)$ the comoving angular diameter distance.

The standardization of SNIa is based on empirical observation that they form a homogeneous class of objects, whose variability can be characterized by two parameters [Tripp (1998)]: the time stretching of the light curve (X_1) and the SNIa color at maximum brightness (C). If we assume that different SNIa with identical colour, shape, and galactic environment have on average the same intrinsic luminosity for all redshifts, the distance modulus can be expressed as

$$\mu_{\text{obs}} = m_B^* - (M_B - \alpha X_1 + \beta C), \quad (2)$$

where m_B^* corresponds to the observed peak magnitude in the B -band rest-frame, while α , β and M_B are nuisance parameters. Although the mechanism is not fully understood, it has been shown [Sullivan et al. (2011); Johansson et al. (2013)] that both β and M_B depend on properties of the host galaxy. In this work we use the joint light-curve analysis from Betoule et al. (2014), where the authors approximately correct for these effects assuming that the absolute magnitude M_B is related to the stellar mass of the host galaxy, M_{stellar} , by a simple step function

$$M_B = \begin{cases} M_B^1 & \text{if } M_{\text{stellar}} < 10^{10} M_{\odot}, \\ M_B^1 + \Delta_M & \text{otherwise,} \end{cases} \quad (3)$$

where M_B^1 and Δ_M are two extra nuisance parameters. The authors also discard the additional dependency of β on the host stellar mass because it does not have a significant impact on the cosmology.

Concerning the errors and the correlations of the measurements, we use the full covariance matrix provided in Betoule et al. (2014), where the authors have considered several statistical and systematic uncertainties, such as the error propagation of the light-curve fit uncertainties, calibration, light-curve model, bias correction, mass step, dust extinction, peculiar velocities, and contamination of non-type Ia supernovae. This covariance matrix depends on the α and β nuisance parameters, so when we sample the parameter space we recompute the covariance matrix at each step.

Allowing for some redshift dependence on the SNIa intrinsic luminosity, the distance modulus can be expressed as

$$\mu_{\text{obs}} = m_B^* - (M_B - \alpha X_1 + \beta C + \Delta m_{\text{evo}}(z)), \quad (4)$$

where $\Delta m_{\text{evo}}(z)$ stands for a nuisance term that accounts for the intrinsic luminosity dependence as a function of the redshift.

Although the mechanism of SNIa detonation is well understood, the difficulty of observing the system before becoming a SNIa leaves enough uncertainty to wonder whether considering a luminosity dependence with the redshift may have an effect on the cosmological conclusions. A varying gravitational constant, or a fine structure constant variation, could generate a luminosity dependence on the redshift, but our approach here is just to consider a phenomenological model to explore the degeneracy of SN distance-dependent effects and the cosmological information. Different phenomenological models have been proposed for $\Delta m_{\text{evo}}(z)$ (see Tutusaus et al. (2017) and references therein). In this work we just consider Model B from Tutusaus et al. (2017), that has also been illustrated in Riess et al. (2018), where $\Delta m_{\text{evo}}(z) = \epsilon z^{\delta}$. A lower δ power contribution models a luminosity evolution dominant at low-redshift, while a higher δ power contribution lead to a luminosity evolution dominating at high-redshift. It is important to notice that δ must be greater than 0, in order not to be degenerate with M_B^1 . When sampling the parameter space we limit $\delta \in [0.2, 2]$.

2.2. Baryon acoustic oscillations

The baryon acoustic oscillations are the characteristic patterns observed in the galaxy distribution of the large-scale structure of the Universe. They are characterized by the length of a standard ruler, r_d , and, in the standard cosmological model, they are originated from sound waves propagating in the early Universe. The BAO scale r_d corresponds then to the comoving sound horizon at the redshift of the baryon drag epoch,

$$r_d = r_s(z_{\text{drag}}) = \int_{z_{\text{drag}}}^{\infty} \frac{c_s(z) dz}{H(z)}, \quad (5)$$

where $z_{\text{drag}} \approx 1060$ and $c_s(z)$ is the sound velocity as a function of the redshift,

$$c_s(z) = \frac{c}{\sqrt{3(1 + R_b(z))}}, \quad \text{with } R_b(z) = \frac{3\rho_b}{4\rho_\gamma}. \quad (6)$$

In this expression ρ_b stands for the baryon density while ρ_γ corresponds to the photon density. Their ratio can be approximated [Eisenstein & Hu (1998)] by $R_b(z) = 3.15 \times 10^4 \Omega_b h^2 \Theta_{2.7}^{-4} (1+z)^{-1}$, with $\Theta_{2.7} = T_{\text{CMB}}/2.7$ K and Ω_b the baryon energy density parameter. In this work we fix the temperature of the CMB to $T_{\text{CMB}} = 2.725$ K [Fixsen (2009)].

However, it is known that models differing from the standard Λ CDM framework may have a value for r_d that is not compatible with $r_s(z_{\text{drag}})$ [Verde et al. (2017b)], and it has also been shown that the computation of r_d may have an effect on the trouble with the Hubble constant H_0 [Bernal et al. (2016)]. Moreover, there has recently been some analyses computing r_d without any dependence on late-time Universe assumptions [Verde et al. (2017a)]. Because of all this, in this work we consider three different methods to include BAO data: either we compute r_d with equation (5), or we let it free, or we include the prior $r_d = 147.4 \pm 0.7$ Mpc from Verde et al. (2017a).

We consider both isotropic and anisotropic measurements of the BAO. The distance scale used for isotropic measurements is given by

$$D_V(z) = \left(r^2(z) \frac{cz}{H(z)} \right)^{1/3}, \quad (7)$$

while for the radial and transverse measurements the distance scales are $r(z)$ and $H(z)$, respectively.

We use the isotropic measurements provided by 6dFGS at $z = 0.106$ [Beutler et al. (2011)] and by SDSS - MGS at $z = 0.15$ [Ross et al. (2015)], as well as the results from WiggleZ at $z = 0.44, 0.6, 0.73$ [Kazin et al. (2014)]. We also consider the anisotropic final results of BOSS DR12 at $z = 0.38, 0.51, 0.61$ [Alam et al. (2017)], and the new anisotropic measurements from the eBOSS DR14 quasar sample [Gil-Marín et al. (2018)] at $z = 1.19, 1.50, 1.83$. These results have been obtained by measuring the redshift space distortions using the power spectrum monopole, quadrupole and hexadecapole. The authors in Gil-Marín et al. (2018) have shown that their results are completely consistent with different methods used for analyzing the same data [Hou et al. (2018); Zarrouk et al. (2018)]. We finally consider the latest results from the combination of the Ly- α forest auto-correlation function [Bautista, J. E. et al. (2017)] and the Ly- α -quasar cross-correlation function [du Mas des Bourboux, H. et al. (2017)] from the complete BOSS survey at $z = 2.4$. We take into account the covariance matrix provided for the measurements of WiggleZ, BOSS DR12, eBOSS DR14, we consider a correlation coefficient of -0.38 for the Ly- α forest measurements, and we assume measurements of different surveys to be uncorrelated. In order to take into account the non-Gaussianity of the BAO observable likelihoods far from the peak, we follow Bassett & Afshordi (2010) by replacing the usual $\Delta\chi_G^2 = -2\ln\mathcal{L}_G$ for a Gaussian likelihood observable by

$$\Delta\chi^2 = \frac{\Delta\chi_G^2}{\sqrt{1 + \Delta\chi_G^4 \left(\frac{S}{N}\right)^{-4}}}, \quad (8)$$

where the ratio S/N stands for the detection significance, in units of σ , of the BAO feature. We consider a detection significance of 2.4σ for 6dFGS, 2σ for SDSS-MGS and WiggleZ, 9σ for BOSS DR12, 4σ for eBOSS DR14, and 5σ for the Ly- α forest.

2.3. Cosmic microwave background

The cosmic microwave background is an extremely powerful source of information due to the high precision of modern data. Furthermore it represents high-redshift data, complementing low-redshift probes. As it was shown in Wang & Mukherjee (2007), a significant part of the information coming from the

CMB can be compacted into a few numbers, the so-called reduced parameters: the scaled distance to recombination R , the angular scale of the sound horizon at recombination ℓ_a , and the reduced density parameter of baryons ω_b . For a flat universe their expressions are given by

$$\begin{aligned} R &\equiv \sqrt{\Omega_m H_0^2} \int_0^{z_{\text{CMB}}} \frac{dz}{H(z)}, \\ \ell_a &\equiv \frac{\pi c}{r_s(z_{\text{CMB}})} \int_0^{z_{\text{CMB}}} \frac{dz}{H(z)}, \\ \omega_b &\equiv \Omega_b h^2, \end{aligned} \quad (9)$$

where z_{CMB} stands for the redshift of the last scattering epoch. In this work we consider the data obtained from the Planck 2015 data release [Planck Collaboration et al. (2016b)], where the compressed likelihood parameters are obtained from the Planck temperature-temperature plus the low- ℓ Planck temperature-polarization likelihoods. We specifically consider the reduced parameters obtained when marginalizing over the amplitude of the lensing power spectrum for the lower values, since it leads to a more conservative approach, together with their covariance matrix.

3. Methodology

In this section we first remind the standard Λ CDM model and we then present the reconstruction method used to obtain the expansion rate as a function of the redshift. We give a detailed explanation of how we introduce each cosmological probe in the analysis, and we finally describe the method used to sample the parameter space.

3.1. The Λ CDM model

The flat Λ CDM model assumes a flat Robertson-Walker metric together with Friedmann-Lemaître dynamics, leading to the comoving angular diameter distance,

$$r(z) = c \int_0^z \frac{dz'}{H(z')}, \quad (10)$$

and the Friedmann-Lemaître equation,

$$E(z)^2 \equiv \frac{H(z)^2}{H_0^2} = \Omega_r(1+z)^4 + \Omega_m(1+z)^3 + (1 - \Omega_r - \Omega_m), \quad (11)$$

where Ω_m (Ω_r) stands for the matter (radiation) energy density parameter. We follow Planck Collaboration et al. (2016a) in computing the radiation contribution as

$$\Omega_r = \Omega_\gamma \left[1 + N_{\text{eff}} \frac{7}{8} \left(\frac{4}{11} \right)^{4/3} \right], \quad (12)$$

where Ω_γ corresponds to the photon contribution

$$\Omega_\gamma = 4 \times 5.6704 \times 10^{-8} \frac{T_{\text{CMB}}^4}{c^3} \frac{8\pi G}{3H_0^2}. \quad (13)$$

In this work we fix the effective number of neutrino-like relativistic degrees of freedom to $N_{\text{eff}} = 3.04$. When we consider

only SNIa data, or SNIa combined with BAO data letting r_d free, we fix the value of H_0 for the radiation contribution on Λ CDM [see equations (12, 13)] to $H_0 = 68 \text{ km s}^{-1} \text{ Mpc}^{-1}$, since there is no sensitivity to H_0 in these cases. However, H_0 is left free for all the other cases and reconstructions in the rest of the work. The remaining parameters when fitting Λ CDM to the data are Ω_m and the corresponding nuisance parameters of the cosmological probes considered (see Table 1).

3.2. Expansion rate reconstruction method

We want our reconstruction to be as model-independent as possible, and we impose a smooth and continuous expansion rate. Several model-independent reconstruction methods have been used in the literature to reconstruct the dark energy equation of state parameter, or even the Hubble parameter. Among them let us mention the principal component analysis [Huterer & Starkman (2003); Crittenden et al. (2009); Liu et al. (2016); Said et al. (2013); Qin et al. (2015)], the Gaussian processes [Clarkson & Zunckel (2010); Holsclaw et al. (2010); Seikel et al. (2012); Yu et al. (2017); Busti et al. (2014); Wang & Meng (2017)], or, very recently, the Weighted Polynomial Regression method [Gómez-Valent & Amendola (2018)]. In this work we follow the approach from Bernal et al. (2016), reconstructing the late-time expansion history by expressing $E(z) \equiv H(z)/H_0$ in piecewise natural cubic splines. When we consider SNIa data alone, $E(z)$ is specified by its values at 5 different “knots” in redshift: $z = 0.1, 0.25, 0.57, 0.8, 1.3$. Therefore, our reconstruction when analyzing SNIa data considers the following set of parameters $\{h_i, \alpha, \beta, M, \Delta_M, \epsilon, \delta\}$ with h_i for $i \in [1, 5]$ being the 5 knots in redshift, $\alpha, \beta, M, \Delta_M$ the standard SNIa nuisance parameters, and ϵ, δ the SNIa intrinsic luminosity evolution parameters.

When BAO data is added into the analysis we consider an extra knot in our reconstruction at $z = 2.4$. We follow two different approaches to include the BAO measurements: first we consider the product $H_0 r_d$ as a free parameter, and secondly we add information coming from the early Universe through the prior on r_d from Verde et al. (2017a), $r_d = 147.4 \pm 0.7 \text{ Mpc}$. In the first case, the set of parameters considered in our reconstruction of $E(z)$ is $\{h_i, \alpha, \beta, M, \Delta_M, H_0 r_d, \epsilon, \delta\}$ with h_i for $i \in [1, 6]$ being the 6 knots in redshift, while in the second case we consider H_0 and r_d separately $\{h_i, \alpha, \beta, M, \Delta_M, H_0, r_d, \epsilon, \delta\}$.

When we finally add the reduced parameters for the CMB we need to specify $E(z)$ up to early-times. In order to do this we add the seventh knot at $z = 2.7$ computed according to a matter dominated model (with flat Robertson-Walker metric and Friedmann-Lemaître dynamics) with free H_0 and Ω_m parameters [see equation (11)], and we extend the model up to very high-redshift. The main idea in this reconstruction is to start at early-times following a matter dominated model (plus radiation and a negligible contribution of dark energy through a cosmological constant) and, when we start to have low-redshift data and a cosmological constant is still negligible with respect to the quantity of matter present in the Universe, we reconstruct $E(z)$ through a cubic spline interpolation; in this way we give our reconstruction the freedom to choose the preferred expansion without specifying a particular model for dark energy. When analyzing the data we consider three different cases, depending on the way of introducing the BAO measurements. First, we consider r_d as a free parameter, while, in a second place, we add the prior on r_d from Verde et al. (2017a). In both cases, the set of parameters that enters into the reconstruction is given by $\{h_i, \alpha, \beta, M, \Delta_M, H_0, r_d, \Omega_m, z_{\text{CMB}}, \omega_b, \epsilon, \delta\}$, and we add the prior on $z_{\text{CMB}} = 1089.90 \pm 0.23$ [Planck Collabora-

tion et al. (2016a)]. As a last case we compute the value of r_d using equation (5). In this case the set of parameters is given by $\{h_i, \alpha, \beta, M, \Delta_M, H_0, \Omega_m, z_{\text{CMB}}, \omega_b, z_{\text{drag}}, \epsilon, \delta\}$, and we add the prior on $z_{\text{drag}} = 1059.68 \pm 0.29$ [Planck Collaboration et al. (2016a)].

In order to test the degeneracy between a SNIa intrinsic luminosity redshift dependence and cosmic acceleration, we consider different cases with and without evolution, so ϵ and δ can be removed from the analysis, and we also consider coasting reconstructions, in which the universe has a late-time constant expansion rate. More specifically, we fix the first 4 knots (3 for SNIa alone) such that $E(z)$ is equal to $(1+z)$ at these points. See Table 1 for a summary of the different cases considered and the cosmological and nuisance parameters present in them.

3.3. Fitting the data

In order to reconstruct the expansion rate as a function of the redshift, we fit the data minimizing the common χ^2 function,

$$\chi^2 = (\mathbf{u} - \mathbf{u}_{\text{data}})^T C^{-1} (\mathbf{u} - \mathbf{u}_{\text{data}}), \quad (14)$$

where \mathbf{u} stands for the model prediction, while \mathbf{u}_{data} and C hold for the observables and their covariance matrix, respectively. We sample the parameter space to minimize this function using the MIGRAD application from the `iminuit` Python package¹, a Python implementation of the former MINUIT Fortran code [James & Roos (1975)], conceived to find the minimum value of a multiparameter function and analyze the shape of the function around the minimum. We use it to extract the best-fit values for the parameters, as well as their errors and the covariance matrix of the parameters.

We also compute the probability that a higher value for the χ^2 occurs for a fit with $\nu = N - k$ degrees of freedom, where N is the number of data points and k is the number of parameters,

$$P(\chi^2, \nu) = \frac{\Gamma\left(\frac{\nu}{2}, \frac{\chi^2}{2}\right)}{\Gamma\left(\frac{\nu}{2}\right)}, \quad (15)$$

where $\Gamma(t, x)$ is the upper incomplete gamma function and $\Gamma(t) = \Gamma(t, 0)$ the complete gamma function. This value provides us with a goodness of fit statistic. A probability close to 1 indicates that it is likely to obtain higher χ^2 values than the minimum found, pointing to a good fit by the model. When we combine different probes, we minimize the sum of the individual χ^2 functions for each probe, i.e., we assume the probes to be uncorrelated.

4. Results

In this section we present the results of the reconstruction of the expansion rate of the Universe as a function of the redshift for different sets of cosmological probes: SNIa, SNIa combined with BAO, and SNIa combined with both BAO and CMB data. We also comment on the linear growth of structures measurements, and the importance of the value of the Hubble constant, H_0 , to draw conclusions on the accelerated expansion of the Universe.

4.1. Case 1: SNIa

We first start considering only SNIa data. We present this case as an illustration of the reconstruction method used. The best-fit

¹ <https://github.com/iminuit/iminuit>

Table 1. Summary of the cosmological probes and parameters present in the different cases considered. The i -index on h_i goes from 1 to 5 for SNIa data alone, while it goes up to 6 when BAO data is included. When working with coasting reconstructions we only consider the last two knots h_i .

Case	Cosmological probes	Cosmological parameters	Nuisance parameters
SNIa	SNIa	h_i	$\alpha, \beta, M, \Delta_M$
SNIa+BAO free $H_0 r_d$	SNIa+BAO	$h_i, H_0 r_d$	$\alpha, \beta, M, \Delta_M$
SNIa+ev+BAO free $H_0 r_d$	SNIa+BAO	$h_i, H_0 r_d$	$\alpha, \beta, M, \Delta_M, \epsilon, \delta$
SNIa+BAO prior r_d	SNIa+BAO	h_i, H_0, r_d	$\alpha, \beta, M, \Delta_M$
SNIa+ev+BAO prior r_d	SNIa+BAO	h_i, H_0, r_d	$\alpha, \beta, M, \Delta_M, \epsilon, \delta$
SNIa+BAO free r_d +CMB	SNIa+BAO+CMB	$h_i, H_0, r_d, \Omega_m, \omega_b$	$\alpha, \beta, M, \Delta_M, z_{\text{CMB}}$
SNIa+ev+BAO free r_d +CMB	SNIa+BAO+CMB	$h_i, H_0, r_d, \Omega_m, \omega_b$	$\alpha, \beta, M, \Delta_M, z_{\text{CMB}}, \epsilon, \delta$
SNIa+BAO prior r_d +CMB	SNIa+BAO+CMB	$h_i, H_0, r_d, \Omega_m, \omega_b$	$\alpha, \beta, M, \Delta_M, z_{\text{CMB}}$
SNIa+ev+BAO prior r_d +CMB	SNIa+BAO+CMB	$h_i, H_0, r_d, \Omega_m, \omega_b$	$\alpha, \beta, M, \Delta_M, z_{\text{CMB}}, \epsilon, \delta$
SNIa+BAO compute r_d +CMB	SNIa+BAO+CMB	$h_i, H_0, \Omega_m, \omega_b$	$\alpha, \beta, M, \Delta_M, z_{\text{CMB}}, z_{\text{drag}}$
SNIa+ev+BAO compute r_d +CMB	SNIa+BAO+CMB	$h_i, H_0, \Omega_m, \omega_b$	$\alpha, \beta, M, \Delta_M, z_{\text{CMB}}, z_{\text{drag}}, \epsilon, \delta$

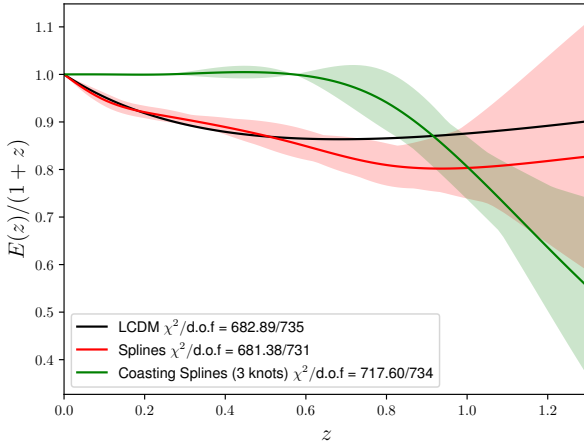


Fig. 1. Reconstruction of the expansion rate, $E(z)/(1+z)$, as a function of the redshift using SNIa data alone. The black line represents the Λ CDM model, while the red band shows the reconstruction with $\Delta\chi^2 = 1$ with respect to the best reconstruction (red line). The green band stands for the reconstruction of a coasting universe at low-redshift. See the text for the details of the reconstruction.

values for the cosmological and nuisance parameters are presented in Table 2 together with the 1σ error bars, and the reconstructions are shown in Fig. 1. We show three different models in this case: the reconstruction through cubic splines (red), the reconstruction for a coasting universe (labelled CS) at low-redshift (fixing the first 3 knots - green), and Λ CDM as a reference (black). We do not consider any SNIa luminosity evolution for the moment. In Table 2 we also provide the reader with the ratio of the χ^2 over the number of degrees of freedom, and the probability $P(\chi^2, \nu)$ from equation (15). In order to obtain the bands for the reconstructions we generate 500 splines from an N -dimensional Gaussian centered at the best-fit values and with the covariance matrix obtained from the fit to the data. We fur-

ther require each spline to have a $\Delta\chi^2$ value smaller or equal than 1 with respect to the best-fit reconstruction.

In Table 2 we can clearly see that all the SNIa nuisance parameters values are compatible for the three models, and that a coasting universe shows a lower expansion rate when we increase the redshift with respect to the standard spline reconstruction. This is confirmed from Fig. 1 where we see that the expansion rate drops above $z \approx 0.8$. We can also observe in this figure that the bands increase when we increase the redshift, as expected, since there are less data points in this region. Comparing the three models, we observe that the spline reconstruction provides a slightly smaller χ^2 value (681.38) than Λ CDM (682.89), but the former has many more parameters in the model, so the ability of these models to fit the data is roughly the same, being slightly better for Λ CDM ($P(\chi^2, \nu) = 0.915$) than the spline reconstruction ($P(\chi^2, \nu) = 0.905$). However, the χ^2 value obtained for the coasting reconstruction (717.60) is much larger than the previous values, which also implies that this model is less able to perfectly fit the data ($P(\chi^2, \nu) = 0.661$). A detailed model comparison is beyond the scope of this work, since we are interested in studying the accelerated expansion of the Universe and the relation it may have with SNIa luminosity, not in proposing a new cosmological model to confront against Λ CDM. However, the coasting reconstruction has a relative probability of $\exp(-\Delta\chi^2/2) \approx 1.4 \times 10^{-6} \%$, showing that a coasting universe at low-redshift is totally excluded, even using SNIa data alone, when SNIa intrinsic luminosity is assumed to be redshift independent. Notice also that, even if we ask the reconstruction to be non-accelerated at low-redshift, it prefers to add some acceleration at earlier times (above $z \approx 0.8$) than just having a constant velocity expansion.

4.2. Case 2: SNIa+BAO

After having shown how the reconstruction method works, and having applied it to SNIa data alone, we focus on the combination of SNIa and BAO data. As it is shown in Table 1 we consider two different ways to combine these data sets: we either let the product $H_0 r_d$ free, or we add a prior on r_d . Since we

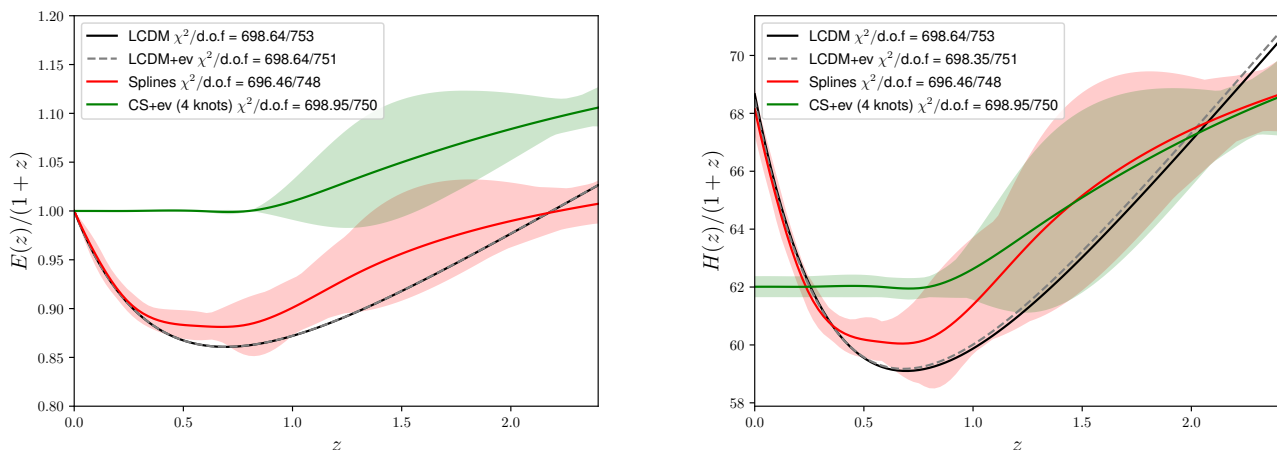


Fig. 2. Reconstruction of the expansion rate, $E(z)/(1+z)$ (left) and $H(z)/(1+z)$ (right), as a function of the redshift using the combination of SNIa and BAO data. In the left panel the data sets have been combined considering $H_0 r_d$ a free parameter, while in the right panel a prior on r_d has been added. In both panels the black and grey lines represent the Λ CDM model (without and with SNIa luminosity evolution, respectively), while the red band shows the reconstruction with $\Delta\chi^2 = 1$ with respect to the best reconstruction (red line). The green band stands for the reconstruction of a coasting universe at low-redshift when SNIa intrinsic luminosity is allowed to vary as a function of the redshift. See the text for the details of the reconstruction.

consider the models with and without SNIa intrinsic luminosity evolution, and we always add Λ CDM as a reference, we finally have 4 different subcases with the corresponding three models per subcase. The best-fit values and errors for the parameters for all these cases are shown in Table 3.

Let us first focus on the case where $H_0 r_d$ is treated as a free parameter. As it was the case with SNIa data alone, all the SNIa nuisance parameters have compatible values for the different models considered. However, the coasting reconstruction now does not show a reduced expansion rate at high-redshift (adding or not SNIa luminosity evolution), due to the addition of the BAO data points above $z \sim 0.8$. We can also see that the value of $H_0 r_d$ obtained from the spline reconstruction is more or less compatible with the one obtained with Λ CDM, but it is lower for the coasting reconstruction, adding SNIa intrinsic luminosity or not. Concerning the ability of the models to fit the data, the χ^2 of the spline reconstruction is always slightly smaller than the Λ CDM one (696.46 against 698.64, and 694.21 against 698.64 when we allow the SNIa luminosity to vary). But as it was the case before, the probability of providing a good fit is roughly the same for both models, being slightly better for Λ CDM (0.911 against 0.922, and 0.912 against 0.914 when we account for evolution). It is also what can be seen in the reconstruction plot on the left panel of Fig. 2. With respect to the coasting reconstruction, we can see in Table 3 that, when SNIa intrinsic luminosity is allowed to vary, we obtain a χ^2 value very close to the Λ CDM one, thus giving also a good probability to correctly fit the data (0.909 against 0.912, for the standard reconstruction, and 0.914, for Λ CDM).

Let us now focus on the combination of SNIa and BAO data with a prior on r_d (two last rows of Table 3 and the right panel of Fig. 2). It allows us to obtain a constraint on H_0 , so we represent in this case the expansion rate by $H(z)/(1+z)$. All the best-fit values for the parameters are very close to the previous case, with nearly the same χ^2 values and the same probabilities, since we have only added one data point and one parameter in the analysis. As before, a coasting universe provides a good fit to the data with a probability of 0.909 against 0.912, for the standard spline

reconstruction, and 0.915 for Λ CDM, when SNIa luminosity is allowed to vary. The interesting result from these cases is that the value found for H_0 for the spline reconstruction is always smaller than the one obtained for Λ CDM, but still compatible, while it is significantly smaller for the coasting reconstruction, as it can be seen in the right plot of Fig. 2. This is consistent with the lower value found for $H_0 r_d$ in the previous cases for the coasting reconstruction.

4.3. Case 3: SNIa+BAO+CMB

As a last case we consider the combination of the three main background expansion cosmological probes: SNIa, BAO, and CMB. We have already presented two different ways to combine SNIa and BAO data, so when we add CMB data we keep this approach and, since we now include the physics of the early Universe, we add a third way consisting on computing the explicit value of r_d . The best-fit values, with the 1σ errors, for the parameters for these three subcases are presented in Table 4, and the corresponding reconstruction in Fig. 3.

Let us start with the combination considering r_d a free parameter. Both assuming the SNIa intrinsic luminosity to be redshift independent or allowing it to vary, the three models provide compatible values for all the parameters except H_0 , which is significantly smaller for the coasting reconstruction, as it was already shown in the combination of SNIa and BAO data, and which is compensated by a larger Ω_m . When SNIa luminosity is allowed to vary, a coasting reconstruction provides roughly the same χ^2 (699.44) as Λ CDM (698.66) with a slightly smaller probability (0.906 against 0.918), showing that a non-accelerated expanding universe can fit the three main background probes when SNIa intrinsic luminosity is allowed to vary.

In a second place we add a prior on r_d . All the best-fit values are compatible between the different models as before, except for H_0 and Ω_m , which are smaller and larger for a coasting reconstruction, respectively, accounting for SNIa luminosity evolution or not. The obtained χ^2 values are very similar, leading to very similar probabilities to correctly fit the data, and they show that

Table 2. Best-fit values with the corresponding 1σ error bars for the cosmological and nuisance parameters of the first case: SNIa data. The values of Λ CDM are added as a reference. The reduced χ^2 and the probability $P(\chi^2, \nu)$ are also provided for the different models.

Case	Model	h_1	h_2	h_3	h_4	h_5	h_6	h_7	h_8	h_9	h_{10}	h_{11}	h_{12}	h_{13}	h_{14}	h_{15}	h_{16}	h_{17}	h_{18}	h_{19}	h_{20}	Ω_m	α	β	M	Δ_M	$\chi^2/\text{d.o.f}$	$P(\chi^2, \nu)$		
SNIa	Λ CDM	—	—	—	—	—	—	—	—	—	—	—	—	—	—	—	—	—	—	—	—	—	—	—	—	—	—	—	—	
	Splines	1.041 ± 0.022	1.141 ± 0.023	1.344 ± 0.071	1.46 ± 0.13	1.90 ± 0.90	—	—	—	—	—	—	—	—	—	—	—	—	—	—	—	—	—	—	—	—	—	—	—	—
	CS (3 knots)	—	—	—	1.69 ± 0.15	1.27 ± 0.58	—	—	—	—	—	—	—	—	—	—	—	—	—	—	—	—	—	—	—	—	—	—	—	—

Table 3. Best-fit values with the corresponding 1σ error bars for the cosmological and nuisance parameters of the second case: SNIa and BAO data. The values of Λ CDM are added as a reference. The reduced χ^2 and the probability $P(\chi^2, \nu)$ are also provided for the different models.

Case	Model	h_1	h_2	h_3	h_4	h_5	h_6	h_7	h_8	h_9	h_{10}	h_{11}	h_{12}	h_{13}	h_{14}	h_{15}	h_{16}	h_{17}	h_{18}	h_{19}	h_{20}	Ω_m	α	β	M	Δ_M	ϵ	δ	$\chi^2/\text{d.o.f}$	$P(\chi^2, \nu)$				
SNIa+BAO free H_{0,r_d}	Λ CDM	—	—	—	—	—	—	—	—	—	—	—	—	—	—	—	—	—	—	—	—	—	—	—	—	—	—	—	—	—				
	Splines	1.050 ± 0.020	1.133 ± 0.020	1.385 ± 0.035	1.591 ± 0.074	2.15 ± 0.14	3.43 ± 0.10	10.040 ± 174	—	—	—	—	—	—	—	—	—	—	—	—	—	—	—	—	—	—	—	—	—	—	—	—		
	CS (4 knots)	—	—	—	—	—	—	—	—	—	—	—	—	—	—	—	—	—	—	—	—	—	—	—	—	—	—	—	—	—	—	—		
SNIa+ev+BAO free H_{0,r_d}	Λ CDM	—	—	—	—	—	—	—	—	—	—	—	—	—	—	—	—	—	—	—	—	—	—	—	—	—	—	—	—	—	—	—		
	Splines	1.118 ± 0.044	1.241 ± 0.065	1.510 ± 0.078	1.77 ± 0.13	2.34 ± 0.18	3.70 ± 0.19	9286 ± 420	—	—	—	—	—	—	—	—	—	—	—	—	—	—	—	—	—	—	—	—	—	—	—	—	—	
	CS (4 knots)	—	—	—	—	—	—	—	—	—	—	—	—	—	—	—	—	—	—	—	—	—	—	—	—	—	—	—	—	—	—	—	—	
SNIa+BAO prior r_d	Λ CDM	—	—	—	—	—	—	—	—	—	—	—	—	—	—	—	—	—	—	—	—	—	—	—	—	—	—	—	—	—	—	—	—	
	Splines	1.050 ± 0.020	1.133 ± 0.019	1.385 ± 0.032	1.591 ± 0.073	2.15 ± 0.14	3.43 ± 0.10	68.1 ± 1.2	147.40 ± 0.70	—	—	—	—	—	—	—	—	—	—	—	—	—	—	—	—	—	—	—	—	—	—	—	—	
	CS (4 knots)	—	—	—	—	—	—	—	—	—	—	—	—	—	—	—	—	—	—	—	—	—	—	—	—	—	—	—	—	—	—	—	—	—
SNIa+ev+BAO prior r_d	Λ CDM	—	—	—	—	—	—	—	—	—	—	—	—	—	—	—	—	—	—	—	—	—	—	—	—	—	—	—	—	—	—	—	—	—
	Splines	1.048 ± 0.021	1.149 ± 0.023	1.410 ± 0.039	1.671 ± 0.095	2.20 ± 0.15	3.46 ± 0.11	62.04 ± 0.55	147.40 ± 0.70	—	—	—	—	—	—	—	—	—	—	—	—	—	—	—	—	—	—	—	—	—	—	—	—	—
	CS (4 knots)	—	—	—	—	—	—	—	—	—	—	—	—	—	—	—	—	—	—	—	—	—	—	—	—	—	—	—	—	—	—	—	—	—

Table 4. Best-fit values with the corresponding 1σ error bars for the cosmological and nuisance parameters of the third case: SNIa, BAO, and CMB data. The values of Λ CDM are added as a reference. The reduced χ^2 and the probability $P(\chi^2, \nu)$ are also provided for the different models.

Case	h_0	h_1	h_2	h_3	h_4	h_5	h_6	t_0	τ_d	Ω_m	$10^7 \omega_b$	σ	β	M	Δ_M	z_{CMB}	z_{drag}	ϵ	δ	$\chi^2/\text{d.o.f.}$	$P(\chi^2, \nu)$
Λ CDM	1.050 ± 0.020	1.133 ± 0.020	1.386 ± 0.034	1.592 ± 0.075	2.14 ± 0.15	3.48 ± 0.10	69.14 ± 0.95	146.2 ± 1.4	0.297 ± 0.011	2.264 ± 0.025	0.1412 ± 0.0066	3.102 ± 0.080	24.110 ± 0.018	24.110 ± 0.018	-0.070 ± 0.023	1090.00 ± 0.23	-	-	-	698.67/754	0.926
SNIa+BAO free r_d +CMB	1.050 ± 0.020	1.133 ± 0.020	1.386 ± 0.034	1.592 ± 0.075	2.14 ± 0.15	3.48 ± 0.10	68.4 ± 1.5	146.7 ± 2.5	0.300 ± 0.015	2.263 ± 0.029	0.1410 ± 0.0066	3.099 ± 0.081	24.120 ± 0.030	24.120 ± 0.030	-0.070 ± 0.023	1090.00 ± 0.23	-	-	-	697.01/748	0.909
CS (4 knots)	-	-	-	-	2.29 ± 0.16	3.795 ± 0.096	62.5 ± 1.1	146.2 ± 2.5	0.359 ± 0.014	2.264 ± 0.029	0.1382 ± 0.0066	3.073 ± 0.080	24.230 ± 0.017	24.230 ± 0.017	-0.077 ± 0.023	1090.00 ± 0.23	-	-	-	740.32/752	0.612
Λ CDM	1.049 ± 0.021	1.149 ± 0.023	1.410 ± 0.039	1.671 ± 0.094	2.18 ± 0.16	3.48 ± 0.10	69.11 ± 0.97	146.2 ± 1.4	0.294 ± 0.012	2.264 ± 0.025	0.1413 ± 0.0066	3.103 ± 0.081	24.110 ± 0.036	24.110 ± 0.036	-0.070 ± 0.023	1090.00 ± 0.23	-	0.085 ± 0.075	0.30 ± 0.39	698.66/752	0.918
SNIa+ev+BAO free r_d +CMB	1.049 ± 0.021	1.149 ± 0.023	1.410 ± 0.039	1.671 ± 0.094	2.18 ± 0.16	3.48 ± 0.10	67.3 ± 1.7	147.5 ± 2.6	0.310 ± 0.017	2.263 ± 0.029	0.1413 ± 0.0066	3.101 ± 0.081	24.110 ± 0.031	24.110 ± 0.031	-0.070 ± 0.023	1090.00 ± 0.23	-	0.094 ± 0.064	2.0 ± 1.6	694.93/746	0.909
CS (4 knots)	-	-	-	-	2.36 ± 0.17	3.783 ± 0.095	62.2 ± 1.1	147.1 ± 2.6	0.364 ± 0.015	2.263 ± 0.029	0.1416 ± 0.0066	3.104 ± 0.081	24.050 ± 0.089	24.050 ± 0.089	-0.070 ± 0.023	1090.00 ± 0.23	-	0.322 ± 0.074	0.4 ± 0.24	699.44/750	0.906
Λ CDM	1.050 ± 0.020	1.133 ± 0.020	1.385 ± 0.034	1.595 ± 0.074	2.166 ± 0.096	3.45 ± 0.10	68.69 ± 0.72	147.20 ± 0.65	0.296 ± 0.0090	2.255 ± 0.021	0.1412 ± 0.0066	3.101 ± 0.080	24.110 ± 0.018	24.110 ± 0.018	-0.070 ± 0.023	1090.00 ± 0.23	-	-	-	699.21/755	0.927
SNIa+BAO prior r_d +CMB	1.050 ± 0.020	1.133 ± 0.020	1.385 ± 0.034	1.595 ± 0.074	2.166 ± 0.096	3.45 ± 0.10	68.2 ± 1.2	147.40 ± 0.68	0.302 ± 0.011	2.262 ± 0.028	0.1410 ± 0.0066	3.099 ± 0.081	24.120 ± 0.030	24.120 ± 0.030	-0.070 ± 0.023	1090.00 ± 0.23	-	-	-	697.07/749	0.913
CS (4 knots)	-	-	-	-	2.35 ± 0.089	3.792 ± 0.095	62.09 ± 0.53	147.30 ± 0.67	0.3644 ± 0.0085	2.261 ± 0.028	0.1382 ± 0.0066	3.073 ± 0.080	24.230 ± 0.017	24.230 ± 0.017	-0.077 ± 0.023	1090.00 ± 0.23	-	-	-	740.51/753	0.620
Λ CDM	1.049 ± 0.021	1.149 ± 0.023	1.410 ± 0.038	1.670 ± 0.092	2.175 ± 0.096	3.48 ± 0.10	68.65 ± 0.75	147.20 ± 0.65	0.299 ± 0.0093	2.254 ± 0.022	0.1413 ± 0.0066	3.102 ± 0.081	24.100 ± 0.036	24.100 ± 0.036	-0.070 ± 0.023	1090.00 ± 0.23	-	0.015 ± 0.073	0.2 ± 1.7	699.17/753	0.920
SNIa+ev+BAO prior r_d +CMB	1.049 ± 0.021	1.149 ± 0.023	1.410 ± 0.038	1.670 ± 0.092	2.175 ± 0.096	3.48 ± 0.10	67.3 ± 1.3	147.40 ± 0.68	0.310 ± 0.013	2.264 ± 0.028	0.1413 ± 0.0066	3.101 ± 0.081	24.110 ± 0.030	24.110 ± 0.030	-0.070 ± 0.023	1090.00 ± 0.23	-	0.094 ± 0.063	2.0 ± 1.6	694.93/747	0.913
CS (4 knots)	-	-	-	-	2.374 ± 0.090	3.782 ± 0.094	62.02 ± 0.53	147.40 ± 0.67	0.3680 ± 0.0085	2.263 ± 0.028	0.1416 ± 0.0066	3.104 ± 0.081	24.050 ± 0.095	24.050 ± 0.095	-0.070 ± 0.023	1090.00 ± 0.23	-	0.322 ± 0.079	0.4 ± 0.25	699.46/751	0.911
Λ CDM	1.050 ± 0.020	1.133 ± 0.020	1.385 ± 0.034	1.595 ± 0.074	2.171 ± 0.096	3.45 ± 0.10	68.35 ± 0.59	147.30 ± 0.67	0.3006 ± 0.0071	2.254 ± 0.022	0.1411 ± 0.0066	3.100 ± 0.080	24.110 ± 0.018	24.110 ± 0.018	-0.070 ± 0.023	1090.00 ± 0.23	-	-	-	699.31/755	0.927
SNIa+BAO compute r_d +CMB	1.050 ± 0.020	1.133 ± 0.020	1.385 ± 0.034	1.595 ± 0.074	2.171 ± 0.096	3.45 ± 0.10	68.1 ± 1.2	147.30 ± 0.67	0.303 ± 0.011	2.261 ± 0.028	0.1410 ± 0.0066	3.099 ± 0.081	24.120 ± 0.030	24.120 ± 0.030	-0.070 ± 0.023	1090.00 ± 0.23	-	-	-	697.09/749	0.912
CS (4 knots)	-	-	-	-	2.362 ± 0.087	3.792 ± 0.094	62.04 ± 0.47	147.30 ± 0.67	0.3635 ± 0.0063	2.260 ± 0.027	0.1382 ± 0.0066	3.073 ± 0.078	24.230 ± 0.017	24.230 ± 0.017	-0.077 ± 0.023	1090.00 ± 0.23	-	-	-	740.55/753	0.620
Λ CDM	1.049 ± 0.020	1.149 ± 0.023	1.410 ± 0.039	1.671 ± 0.090	2.180 ± 0.096	3.48 ± 0.10	68.31 ± 0.60	147.30 ± 0.67	0.3010 ± 0.0073	2.253 ± 0.022	0.1413 ± 0.0066	3.103 ± 0.081	24.100 ± 0.036	24.100 ± 0.036	-0.070 ± 0.023	1090.00 ± 0.23	-	0.019 ± 0.073	0.2 ± 1.8	699.24/753	0.920
SNIa+ev+BAO compute r_d +CMB	1.049 ± 0.020	1.149 ± 0.023	1.410 ± 0.039	1.671 ± 0.090	2.180 ± 0.096	3.48 ± 0.10	67.3 ± 1.3	147.30 ± 0.67	0.310 ± 0.012	2.263 ± 0.028	0.1413 ± 0.0066	3.101 ± 0.081	24.110 ± 0.030	24.110 ± 0.030	-0.070 ± 0.023	1090.00 ± 0.23	-	0.094 ± 0.063	2.0 ± 1.4	694.93/747	0.913
CS (4 knots)	-	-	-	-	2.380 ± 0.091	3.782 ± 0.094	61.98 ± 0.50	147.30 ± 0.67	0.3657 ± 0.0065	2.262 ± 0.028	0.1416 ± 0.0066	3.104 ± 0.081	24.050 ± 0.095	24.050 ± 0.095	-0.070 ± 0.023	1090.00 ± 0.23	-	0.322 ± 0.078	0.4 ± 0.25	699.47/751	0.911

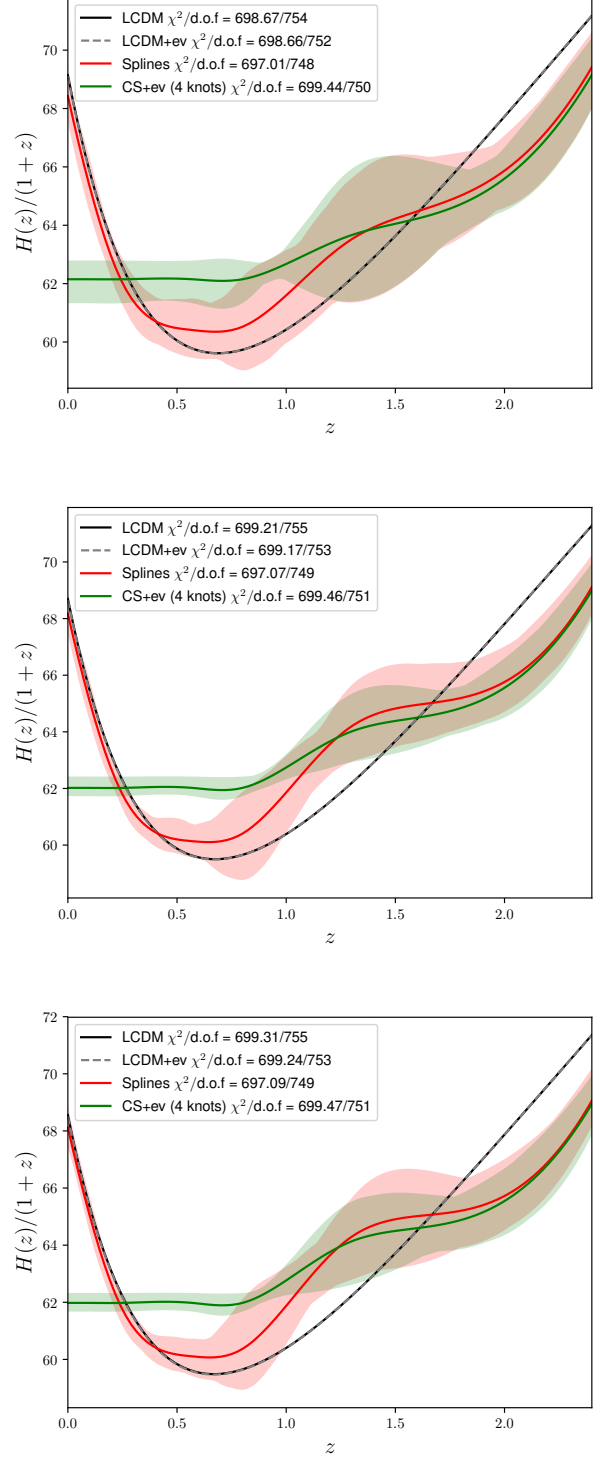


Fig. 3. Reconstruction of the expansion rate, $H(z)/(1+z)$, as a function of the redshift using the combination of SNIa, BAO, and CMB data. In the top panel the data sets have been combined considering r_d a free parameter, while in the central panel a prior on r_d has been used, and it has been explicitly computed in the bottom panel. In all panels the black and grey lines represent the Λ CDM model (without and with SNIa luminosity evolution, respectively), while the red band shows the reconstruction with $\Delta\chi^2 \leq 1$ with respect to the best reconstruction (red line). The green band stands for the reconstruction of a coasting universe at low-redshift when SNIa intrinsic luminosity is allowed to vary as a function of the redshift. See the text for the details of the reconstruction.

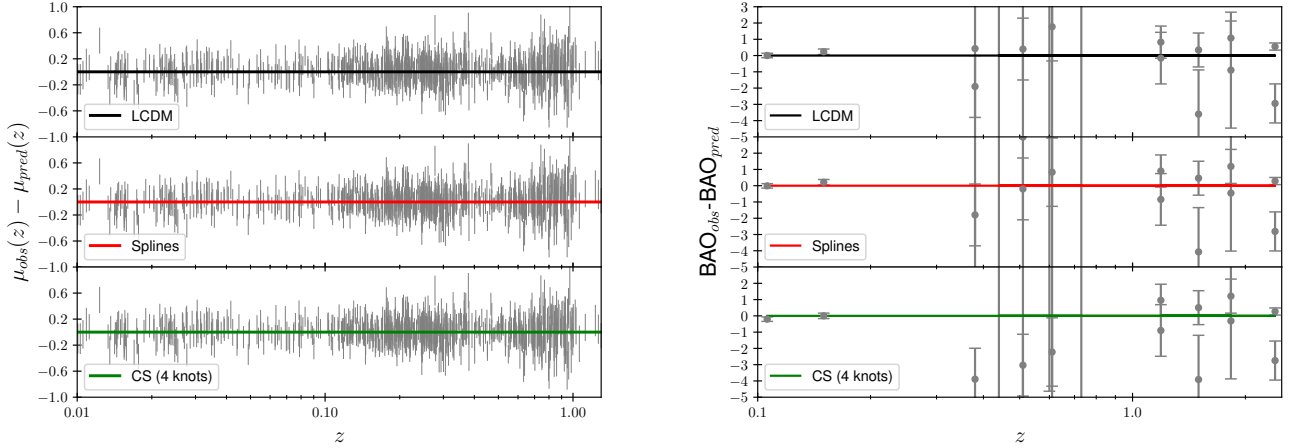


Fig. 4. Prediction of the different models, Λ CDM, spline reconstruction, and coasting reconstruction with SNIa intrinsic luminosity evolution, for the SNIa and BAO observables. The predictions have been computed using the best-fit values for the parameters obtained from the fit of the combination SNIa+BAO+CMB computing r_d explicitly. *Left plot:* Residuals of the SNIa distance modulus for the three different models: Λ CDM (black top panel), spline reconstruction (red central panel), and coasting reconstruction (green bottom panel). The residuals have been normalized with respect to the prediction for each model. *Right plot:* Residuals of the BAO measurements following the same colour convention as in the left panel. The residuals have been normalized with respect to the prediction for each model.

Table 5. Prediction of the different models for the CMB quantities R , ℓ_a , ω_b , for the combination of SNIa, BAO, and CMB data computing r_d explicitly, and accounting for SNIa intrinsic luminosity evolution as a function of the redshift when dealing with a coasting reconstruction. The observed values are added as a reference.

	Observed	Λ CDM	Splines	CS (4 knots)+ev
R	1.7382 ± 0.0088	1.7414	1.7385	1.7382
ℓ_a	301.63 ± 0.15	301.68	301.67	301.65
$10^2 \omega_b$	2.262 ± 0.029	2.254	2.261	2.262

a coasting reconstruction can correctly fit the data when SNIa luminosity evolution is accounted for. In the last place we compute r_d using equation (5). All the best-fit values are compatible with the previous results, and compatible between the different models, except for H_0 and Ω_m . It is also the case for the χ^2 values and the corresponding probabilities. We conclude that a non-accelerated universe can correctly fit the three main background probes when we account for a redshift dependence in the intrinsic luminosity of SNIa.

For completeness, we present in Fig. 4 the residuals to SNIa and BAO observations for three different models: Λ CDM (black), the reconstruction through cubic splines (red), and the non-accelerated model using a coasting reconstruction (green) taking into account SNIa intrinsic luminosity evolution. We also provide the predictions for the CMB quantities R , ℓ_a , and ω_b in Table 5. All these predictions have been computed using the best-fit values for the parameters obtained from the global fit to the combination of SNIa, BAO, and CMB data, computing explicitly the value of r_d using equation (5). From these results we can graphically see that all three models are perfectly able to fit the data; including the coasting reconstruction with SNIa luminosity evolution. As it can be seen in Table 4, a different approach when combining SNIa, BAO, and CMB data gives nearly

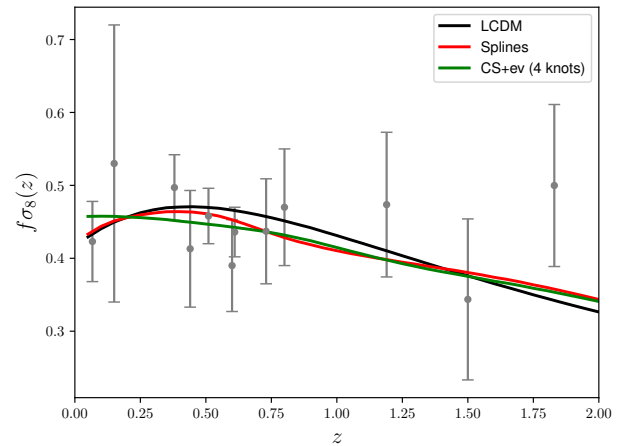


Fig. 5. Prediction of the different models, Λ CDM, spline reconstruction, and coasting reconstruction with SNIa intrinsic luminosity evolution, for the growth of matter perturbations $f\sigma_8$ observable. The predictions have been computed using the best-fit values for the parameters obtained from the fit of the combination SNIa+BAO+CMB computing r_d explicitly. Therefore, it is not a fit to the $f\sigma_8$ measurements. We follow the same colour legend as in the previous figures: black for Λ CDM, red for the spline reconstruction, and green for the coasting reconstruction.

the same values for the parameters, which leads to nearly the same predictions.

4.4. Growth rate

The measurements of the growth rate of matter perturbations offer an additional constraint on cosmological models. Their value depend on the theory of gravity used and it is well known that there are identical background evolutions with different growth rates [Piazza et al. (2014)]. Defining the linear growth factor of

matter perturbations as the ratio between the linear density perturbation and the energy density, $D \equiv \delta\rho_m/\rho_m$, we can derive the standard second order differential equation for D [Peebles (1993)]

$$\ddot{D} + 2H\dot{D} - 4\pi G\rho_m D = 0, \quad (16)$$

where the dot stands for differentiation over the cosmic time. Neglecting second order corrections, this differential equation can be rewritten with derivatives over the scale factor [Dodelson (2003)]

$$D''(a) + \left[\frac{3}{a} + \frac{H'(a)}{H(a)} \right] D'(a) - \frac{3}{2} \Omega_m \frac{H_0^2}{H^2(a)} \frac{D(a)}{a^5} = 0, \quad (17)$$

which is valid under the assumption that dark energy cannot be perturbed and does not interact with dark matter. We can now define the growth factor as

$$f(a) \equiv \frac{d \ln D}{d \ln a}, \quad (18)$$

and then compute the observable weighted growth rate $f\sigma_8$ as

$$f\sigma_8(z) = f(z) \cdot \left(\sigma_{8\text{Planck}} \frac{D(z)}{D_{\text{Planck}}(0)} \right), \quad (19)$$

where $\sigma_{8\text{Planck}}$ stands for the observed value of the root mean square mass fluctuation amplitude on scales of $8h^{-1}$ Mpc at redshift $z = 0$ (fixed to 0.8159 in this work [Planck Collaboration et al. (2016a)]), and D_{Planck} represents the Λ CDM Planck growth rate [Planck Collaboration et al. (2016a)]. In this work we consider the measurements of the weighted growth rate from the 6dFGS survey [Beutler et al. (2012)], the WiggleZ survey [Blake et al. (2012)], and the VIPERS survey [de la Torre et al. (2013)], as well as the different SDSS projects: SDSS-II MGS DR7 [Howlett et al. (2015)] (with the main galaxy sample of the seventh data release), SDSS-III BOSS DR12 [Alam et al. (2017)] (with the LRGs from the 12th BOSS data release), and SDSS-IV DR14Q [Gil-Marín et al. (2018)] (with the latest quasar sample of eBOSS). We have not included this data set in our fitting analysis for simplicity, but we show in Fig. 5 that, using the best-fit values for the parameters from the SNIa+BAO+CMB fit, the prediction for the three models considered (Λ CDM, spline reconstruction, and coasting reconstruction with SNIa luminosity evolution) is in very good agreement with the observations. Notice that the values for the parameters used in Fig. 5 have been obtained computing the value of r_d , but the results are equivalent using the other approaches for the combination of our three main data sets.

4.5. The Hubble constant

The Hubble constant, H_0 , is one of the most important parameters in modern cosmology, since it is used to construct time and distance cosmological scales. It was first measured by Hubble to be roughly 500 km/s/Mpc [Hubble (1929)]. Current data supports a value for H_0 close to 70 km/s/Mpc. However, nearly 100 years later there is still no consensus on its value. Local measurements already show some tension on the results depending on the calibration of SNIa distances [Riess et al. (2018); Tamman, G. A. & Reindl, B. (2013)]. Moreover, there is also some

tension between the direct measurement of H_0 and the value inferred from the CMB assuming a Λ CDM model [Planck Collaboration et al. (2016a)]. There has been many attempts in the literature to solve this discrepancy both from an observational and a theoretical perspective [see Bernal et al. (2016); Gómez-Valent & Amendola (2018) and references therein for a detailed discussion on the trouble with H_0]. In this work we consider two very recent model independent measurements of H_0 in order to check its effect on the conclusions we can draw concerning the cosmic acceleration. We first consider the value obtained from the Hubble Space Telescope observations in Riess et al. (2018) (R18 in the following), $H_0 = 73.45 \pm 1.66$ km/s/Mpc. We then consider the value obtained with Gaussian Processes using SNIa data, and constraints on $H(z)$ from cosmic chronometers in Gómez-Valent & Amendola (2018) (GVA18 in the following), $H_0 = 67.06 \pm 1.68$ km/s/Mpc. This last value is closer to the one derived with an ‘‘inverse distance ladder’’ approach in Aubourg et al. (2015), $H_0 = 67.3 \pm 1.1$, where the measurement assumes standard pre-recombination physics but is insensitive to dark energy or space curvature assumptions. It is also closer to the value derived from the CMB observations using a flat Λ CDM model, $H_0 = 67.51 \pm 0.64$ [Planck Collaboration et al. (2016a)].

In Fig. 6 we represent the profile likelihood (assuming Gaussian likelihoods) for both the observed values of H_0 , R18 (black) and GVA18 (blue), and the values derived from the non-accelerated reconstruction for the combination SNIa+BAO+CMB taking into account the SNIa intrinsic luminosity evolution. We present the three values obtained for the three approaches followed when combining the data sets: consider r_d a free parameter (green), add a prior on it (yellow), or compute it explicitly (purple). From the figure alone it is clear that the H_0 value for the non-accelerated reconstruction is in tension with R18 at more than 5σ , independently of the approach used when combining the data sets. More precisely, a non-accelerated reconstruction is ruled out if we consider the R18 measurement at 5.65σ (free r_d , $H_0 = 62.2 \pm 1.1$), 6.56σ (prior r_d , $H_0 = 62.02 \pm 0.53$), or 6.62σ (compute r_d , $H_0 = 61.98 \pm 0.50$), showing that, with the R18 measurement, cosmic acceleration is proven even if some astrophysical systematics evolving with the redshift modify the intrinsic luminosity of SNIa. However, we can also see from the figure that if we consider the measured value from the Gaussian Processes, a non-accelerated reconstruction shows a bit less than a 3σ tension. More precisely, there is a tension of 2.42σ (free r_d), 2.86σ (prior r_d), or 2.90σ (compute r_d). In this case, the measured value of H_0 points towards ruling out these reconstructions, but the tension is still far from the 5σ threshold.

5. Conclusions

In this paper we have addressed the question whether relaxing the standard assumption that SNIa intrinsic luminosity does not depend on the redshift may have an impact on the conclusions that can be drawn on the accelerated nature of the expansion of the Universe. Although there is no theoretically motivated model for this luminosity evolution, it has not been proven that two SNIa in two galaxies with the same light-curve, colour, and host stellar mass have the same intrinsic luminosity independently of the redshift. Moreover, with this kind of analysis we can distinguish between the effect of unknown astrophysical systematics varying with the redshift and the cosmological information.

The impact of SNIa luminosity evolution on our cosmological knowledge has already been addressed before [Wright (2002); Drell et al. (2000); Linden et al. (2009); Nordin et al. (2008); Fer-

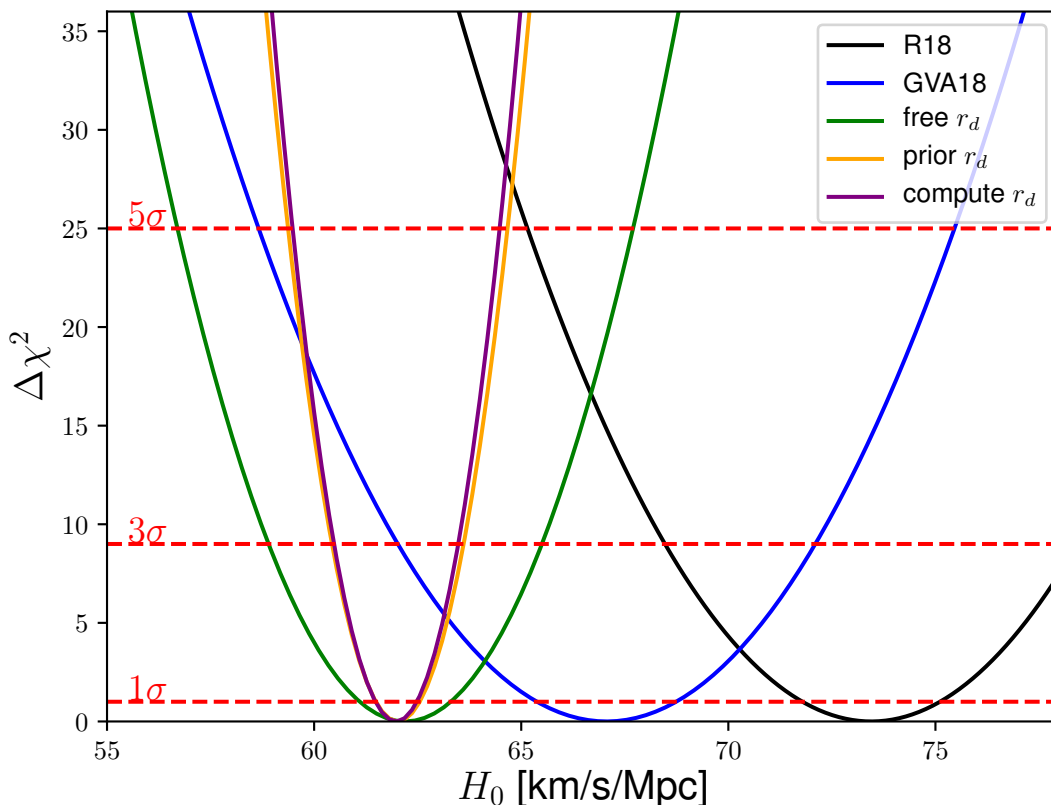


Fig. 6. Profile likelihood (assuming Gaussian likelihoods) of different values for the Hubble constant. The black line corresponds to the value measured from the HST (R18), while the blue one stands for the measured value from SNIa and $H(z)$ data using Gaussian Processes (GVA18). The other three profiles represent the predicted value from a non-accelerated reconstruction with different approaches to combine the three main data sets of this work (SNIa, BAO, and CMB): consider r_d a free parameter (green), add a prior on it (yellow), or compute it explicitly (purple). The 1σ , 3σ , and 5σ lines are represented as a reference.

ramacho et al. (2009); Tutusaus et al. (2016, 2017)], but in this work we have extended the analysis by including the physics of the early Universe ($z \approx 1000$), and thus considering the main background cosmological probes: SNIa, BAO, and the CMB. In order to be as general as possible, we have not imposed a cosmological model, but we have reconstructed the expansion rate of the Universe using a cubic spline interpolation.

We have first applied, as an illustration of the method, the reconstruction to SNIa data alone with the standard SNIa luminosity independence assumption. We have shown that with this assumption cosmic acceleration is definitely preferred against a local non-accelerated universe.

In a second step we have added the latest BAO data to our analysis. We have considered two different ways to combine it with SNIa data: either we have considered $H_0 r_d$ as a free parameter, or we have added a prior on r_d coming from CMB observations, without any dependence on late-time Universe assumptions. In both cases we have seen that a non-accelerated universe is able to fit the data nearly as nicely as Λ CDM, when we allow the SNIa intrinsic luminosity to vary as a function of the redshift.

Next, we have extended the data sets in the analysis by adding the information coming from the CMB through the reduced parameters. In order to deal with this information we have been forced to specify the model up to very high redshifts. We

have decided to follow a matter dominated model (plus radiation and a negligible dark energy contribution in the form of a cosmological constant) from the early Universe down to $z \approx 3$, where we start to have low-redshift data. We have then coupled the model to our spline reconstruction. In other words, we consider a matter-radiation dominated model at the early Universe and, when we start to have low-redshift data and a cosmological constant is still negligible, we allow the expansion rate to vary freely without specifying any dark energy model. When adding the CMB data we follow three different approaches: treat r_d as a free parameter, add a prior on it, or compute it assuming that the BAO and the CMB share the same physics. In all three cases we have seen that a non-accelerated model is able to nicely fit the data, when SNIa intrinsic luminosity is allowed to vary, including the information on the early Universe coming from the CMB.

For simplicity we have not added the $f\sigma_8$ measurements for the growth rate of matter perturbations, but we have checked that using the best-fit values from the global fit SNIa+BAO+CMB we are able to correctly predict the latest $f\sigma_8$ measurements.

After having seen that if SNIa intrinsic luminosity does depend on the redshift, the main cosmological probes are not able to rule out a non-accelerated model, we focus on the impact that the Hubble constant may have on this question. We have consid-

ered two different model independent recent measurements of H_0 : 73.45 ± 1.66 km/s/Mpc (R18) from Riess et al. (2018), and 67.06 ± 1.68 km/s/Mpc (GVA18) from Gómez-Valent & Amendola (2018). We have shown that if we consider the R18 value, cosmic acceleration is proven at more than 5.65σ for a general expansion rate reconstruction [for which we get $H_0 = 62.2 \pm 1.1$ (free r_d), $H_0 = 62.02 \pm 0.53$ (prior r_d), and $H_0 = 61.98 \pm 0.50$ (compute r_d)], even if SNIa intrinsic luminosity varies as a function of the redshift due to any astrophysical unknown systematic. It is important to say, though, that if we consider the GVA18 value, a non-accelerated reconstruction for the expansion rate is at a 3σ tension with the measurement, but still below the 5σ detection.

In conclusion, if SNIa intrinsic luminosity varies as a function of the redshift, a non-accelerated universe is able to correctly fit all the main background probes. However, the value of H_0 turns out to be a key ingredient in the conclusions we can draw concerning the cosmic acceleration. If we take it into account we are close to claim an accelerated expansion of the Universe using an approach very independent of the cosmological model assumed, and even if SNIa intrinsic luminosity varies. A final consensus on a direct measurement of H_0 and its precision will be decisive to finally prove the cosmic acceleration independently of the cosmological model and any redshift dependent astrophysical systematic that may remain in the SNIa analysis.

Acknowledgements. We thank Adam G. Riess and Daniel L. Shafer for very fruitful comments which helped to noticeably improve this work. This work has been carried out thanks to the support of the OCEVU Labex (ANR-11-LABX-0060) and of the Excellence Initiative of Aix-Marseille University - A*MIDEX, part of the French “Investissements d’Avenir” programme.

References

- Alam, S., Ata, M., Bailey, S., et al. 2017, MNRAS, 470, 2617
- Aubourg, E., Bailey, S., Bautista, J. E., et al. 2015, Phys. Rev. D, 92, 123516
- Bassett, B. A. & Afshordi, N. 2010, ArXiv e-prints [arXiv:1005.1664]
- Bautista, J. E., Busca, N. G., Guy, J., et al. 2017, A&A, 603, A12
- Bernal, J. L., Verde, L., & Riess, A. G. 2016, JCAP, 10, 019
- Betoule, M., Kessler, R., Guy, J., et al. 2014, A&A, 568, A22
- Beutler, F., Blake, C., Colless, M., et al. 2011, MNRAS, 416, 3017
- Beutler, F., Blake, C., Colless, M., et al. 2012, MNRAS, 423, 3430
- Blake, C., Brough, S., Colless, M., et al. 2012, MNRAS, 425, 405
- Busti, V. C., Clarkson, C., & Seikel, M. 2014, MNRAS: Letters, 441, L11
- Clarkson, C. & Zunckel, C. 2010, Phys. Rev. Lett., 104, 211301
- Crittenden, R. G., Pogosian, L., & Zhao, G.-B. 2009, JCAP, 12, 025
- Dam, L. H., Heinesen, A., & Wiltshire, D. L. 2017, MNRAS, 472, 835
- de la Torre, S., Guzzo, L., Peacock, J. A., et al. 2013, A&A, 557, A54
- Dodelson, S. 2003, Academic Press
- Drell, P. S., Lored, T. J., & Wasserman, I. 2000, ApJ, 530, 593
- du Mas des Bourboux, H., Le Goff, J.-M., Blomqvist, M., et al. 2017, A&A, 608, A130
- Eisenstein, D. J. & Hu, W. 1998, ApJ, 496, 605
- Ferramacho, L. D., Blanchard, A., & Zolnierowski, Y. 2009, A&A, 499, 21
- Fixsen, D. J. 2009, ApJ, 707, 916
- Gil-Marín, H., Guy, J., Zarrouk, P., et al. 2018, ArXiv e-prints [arXiv:1801.02689]
- Gómez-Valent, A. & Amendola, L. 2018, ArXiv e-prints [arXiv:1802.01505]
- Haridasu, B. S., Luković, V. V., D’Agostino, R., & Vittorio, N. 2017, A&A, 600, L1
- Holsclaw, T., Alam, U., Sansó, B., et al. 2010, Phys. Rev. D, 82, 103502
- Hou, J., Sánchez, A. G., Scoccimarro, R., et al. 2018, ArXiv e-prints [arXiv:1801.02656]
- Howlett, C., Ross, A. J., Samushia, L., Percival, W. J., & Manera, M. 2015, MNRAS, 449, 848
- Hubble, E. 1929, Proceedings of the National Academy of Sciences, 15, 168
- Huterer, D. & Starkman, G. 2003, Phys. Rev. Lett., 90, 031301
- James, F. & Roos, M. 1975, Comput. Phys. Commun., 10, 343
- Johansson, J., Thomas, D., Pforr, J., et al. 2013, MNRAS, 435, 1680
- Kazin, E. A., Koda, J., Blake, C., et al. 2014, MNRAS, 441, 3524
- Lin, H.-N., Li, X., & Sang, Y. 2017, ArXiv e-prints [arXiv:1711.05025]
- Linden, S., Virey, J.-M., & Tilquin, A. 2009, A&A, 506, 1095
- Liu, Z.-E., Yu, H.-R., Zhang, T.-J., & Tang, Y.-K. 2016, Physics of the Dark Universe, 14, 21
- Lonappan, A. I., Kumar, S., Ruchika, Dinda, B. R., & Sen, A. A. 2017, ArXiv e-prints [arXiv:1707.00603]
- Luković, V. V., Haridasu, B. S., & Vittorio, N. 2018, ArXiv e-prints [arXiv:1801.05765]
- Nielsen, J. T., Guffanti, A., & Sarkar, S. 2016, Nature Sci. Rep., 6, 35596
- Nordin, J., Goobar, A., & Jönsson, J. 2008, JCAP, 02, 008
- Peebles, P. 1993, Princeton Univ. Press, Princeton New Jersey
- Perlmutter, S., Aldering, G., Goldhaber, G., et al. 1999, ApJ, 517, 565
- Piazza, F., Steigerwald, H., & Marinoni, C. 2014, JCAP, 05, 043
- Planck Collaboration, Ade, P. A. R., Aghanim, N., et al. 2016a, A&A, 594, A13
- Planck Collaboration, Ade, P. A. R., Aghanim, N., et al. 2016b, A&A, 594, A14
- Qin, H.-F., Li, X.-B., Wan, H.-Y., & Zhang, T.-J. 2015, ArXiv e-prints [arXiv:1501.02971]
- Riess, A. G., Casertano, S., Yuan, W., et al. 2018, ArXiv e-prints [arXiv:1801.01120]
- Riess, A. G., Filippenko, A. V., Challis, P., et al. 1998, Astron. J., 116, 1009
- Riess, A. G., Rodney, S. A., Scolnic, D. M., et al. 2018, ApJ, 853, 126
- Ringermacher, H. I. & Mead, L. R. 2016, ArXiv e-prints [arXiv:1611.00999]
- Ross, A. J., Samushia, L., Howlett, C., et al. 2015, MNRAS, 449, 835
- Rubin, D. & Hayden, B. 2016, ApJ, 833, L30
- Said, N., Baccigalupi, C., Martinelli, M., Melchiorri, A., & Silvestri, A. 2013, Phys. Rev. D, 88, 043515
- Seikel, M., Clarkson, C., & Smith, M. 2012, JCAP, 06, 036
- Shariff, H., Jiao, X., Trotta, R., & van Dyk, D. A. 2016, ApJ, 827, 1
- Sullivan, M., Guy, J., Conley, A., et al. 2011, ApJ, 737, 102
- Tammann, G. A. & Reindl, B. 2013, A&A, 549, A136
- Tripp, R. 1998, A&A, 331, 815
- Tutusaus, I., Lamine, B., Blanchard, A., et al. 2016, Phys. Rev. D, 94, 103511
- Tutusaus, I., Lamine, B., Dupays, A., & Blanchard, A. 2017, A&A, 602, A73
- Verde, L., Bellini, E., Pigozzo, C., Heavens, A. F., & Jimenez, R. 2017a, JCAP, 04, 023
- Verde, L., Bernal, J. L., Heavens, A. F., & Jimenez, R. 2017b, MNRAS, 467, 731
- Wang, D. & Meng, X. 2017, Science China Physics, Mechanics, and Astronomy, 60, 110411
- Wang, Y. & Mukherjee, P. 2007, Phys. Rev. D, 76, 103533
- Wright, E. L. 2002, ArXiv e-prints [astro-ph/0201196]
- Yu, H., Ratra, B., & Wang, F.-Y. 2017, ArXiv e-prints [arXiv:1711.03437]
- Zarrouk, P., Burtin, E., Gil-Marín, H., et al. 2018, ArXiv e-prints [arXiv:1801.03062]